Solar occultation measurement of mesospheric ozone by SAGE III/ISS: Impact of variations along the line of sight caused by photochemistry

Murali Natarajan [1], Robert Damadeo [1], David Flittner [1]

[1] Science Directorate, NASA Langley Research Center, 21 Langley Blvd., Mail Stop 401-B, Hampton, VA 23681, USA.

Correspondence to: Murali Natarajan (murali.natarajan@nasa.gov)

Abstract. Twilight gradients in the concentration of atmospheric species with short photochemical lifetimes influence the transmission data obtained in a solar occultation instrument like the Stratospheric Aerosol and Gas Experiment III aboard the International Space Station (SAGE III/ISS). These photochemically induced changes result in nonlinear asymmetries in the species distribution near the tangent altitude along the line of sight (LOS). The bias introduced by neglecting the effects of twilight variations in the retrieval of mesospheric ozone is the focus of this study. O_3 in the mesosphere exhibits large variations near the terminator during sunrise and sunset based on current understanding of the photochemistry of this altitude region. The algorithm used in the SAGE III/ISS standard retrieval procedure for mesospheric ozone does not include the effects of these gradients. This study illustrates a method for implementing a correction scheme to account for the twilight variations in mesospheric O_3 and gives an estimate of the bias in the standard retrieval. We use the results from a diurnal photochemical model

conducted at different altitudes to develop a database of ratios of mesospheric O_3 at different solar zenith angles (SZA) around 90° to O_3 at a SZA of 90° for both sunrise and sunset conditions. These ratios are used to scale the O_3 at levels above the tangent altitude for appropriate SZA in the calculation of the optical depth along the LOS. In general, the impact of the corrections due to twilight variations is to increase the contribution of the overlying layers to the optical depth thereby reducing the retrieved O_3 concentration at the tangent altitude. We find that at sunrise the retrieved mesospheric O_3 including the diurnal corrections is lower by more than 30% compared to the archived O_3. We show the results obtained for different latitudes and seasons. In addition, for nearly collocated sunrise and sunset scans, we note that these corrections lead to better qualitative agreement in the sunrise to sunset O_3 ratio with the photochemical model prediction.

1 Introduction

The solar occultation measurement technique has been the workhorse among various methods used for monitoring the composition of the earth's atmosphere for over 4 decades. This is evidenced by many successful experiments such as SAGE, SAGE II, Halogen Occultation Experiment (HALOE), Atmospheric Trace Molecule Spectroscopy (ATMOS), Atmospheric Chemistry Experiment – Fourier Transform Spectrometer (ACE-FTS), Polar Ozone and Aerosol Measurement (POAM), SAGE III/M3M and SAGE III/ISS. Major advantages of this technique include high signal to noise ratio, high vertical resolution, and long-term accuracy provided by the 'self-calibrating' nature of the instrument operation. Limited global coverage ranks high among the disadvantages of this method. In the occultation experiments, the absorption of solar

radiance measured by the instrument as a function of tangent height altitude or pressure is related to the optical depth and hence the abundance of the species along the line of sight (LOS). The bulk of the absorption, in general, occurs around the tangent point because of the exponential decrease in atmospheric density with altitude and due to the slant path determined by the spherical geometry. Algorithms used in standard retrievals assume that the species distribution in atmospheric layers is homogeneous and, therefore, the variation along the LOS is symmetrical around the tangent point location. The column along the LOS is then made up of species concentrations at the tangent altitude and the layers above corresponding to a SZA of 90°. This assumption is quite valid for species such as CH_4, H_2O, and stratospheric O_3 because of their long photochemical lifetimes and the absence of chemically induced diurnal variations. In the case of species with short lifetimes, the sudden changes in the photolysis rates near day/night terminator trigger rapid variations in the concentration as a function of SZA. These variations result in nonlinear asymmetry along the LOS. In this case, the column along the LOS is made up of species concentration at a SZA of 90° at the tangent altitude and those from the layers above at SZA different from 90° on either side of the tangent point.

The influence of twilight variations in NO and ClO on the interpretation of solar occultation measurements was described by Boughner et al. (1980). Correction factors based on photochemical models, as discussed in the above study, have been routinely applied in the retrievals of stratospheric NO and NO_2 profiles in HALOE (Gordley et al., 1996; Russell et al., 1988) and in ATMOS (Newchurch et al., 1996). Brohede et al. (2007) described the role of diurnal variations in the retrieval of NO_2 from OSIRIS measurements. The algorithm used in the retrieval of NO_2 in SAGE, SAGE II, SAGE III/M3M, and SAGE III/ISS neglects the twilight

68 variations. A recent study of the NO_2 retrieval from SAGE III/ISS by Dubé et al. (2021)
69 describes the importance of considering the diurnal variations along the LOS.
70
71 Mesospheric O_3 is also characterized by short photochemical lifetimes and steep twilight
72 gradients and, therefore, it is a potential candidate species requiring appropriate corrections in a
73 retrieval from solar occultation instruments. Natarajan et al. (2005) noted that the diurnal
74 correction factors used in the retrieval of mesospheric ozone from HALOE (Version 19) needed
75 to be updated. They derived new factors from a diurnal photochemical model of mesospheric
76 ozone and illustrated the impact of the corrections using a small subset of retrieved HALOE
77 mesospheric O_3 profiles. In the present study, we describe the application of similar corrections
78 to the SAGE III/ISS retrieval of mesospheric O_3. Table 1 of the Data Product User's Guide for
79 SAGE III/ISS (2021) lists the release status of mesospheric O_3 data as a Beta version that is yet
80 to be validated, because it is still potentially impacted by spectral stray light within the
81 instrument. Our goal is to quantify the impact of the corrections on the archived data and to see
82 whether the changes can support other known criteria. A description of the mesospheric O_3
83 variations under twilight conditions as calculated with a diurnal photochemical model is given in
84 section 2. The occultation geometry and the diurnal correction factors for mesospheric O_3 are
85 described in section 3. Results from the application of the factors to correct the archived data are
86 discussed in section 4. We also include the results from an approximate retrieval using the
87 archived transmission data with and without diurnal corrections. A comparison of zonally
88 averaged O_3 profiles with scaled data for the same period from the Microwave Limb Sounder
89 (MLS) instrument on Aura satellite is described in the next section. This is followed by a
90 discussion of sunrise to sunset mesospheric O_3 ratios using appropriate collocated scans and a

comparison to theoretical values. The final summary section reiterates the importance of corrections for photochemically induced twilight mesospheric O_3 variations in solar occultation retrievals.

2 Mesospheric O_3 variations at sunrise/sunset

We use a time-dependent, one-dimensional photochemical model to obtain the diurnal variation in mesospheric O_3. A detailed description of the model used in this study is given in Natarajan et al. (2005). This version of the model extends from 56 km to 100 km at 1 km intervals. The photochemical reaction scheme, shown in the appendix, includes reactions involving species from the Oxygen, Hydrogen, and Nitrogen families. Chlorine and Bromine reactions do not play a significant role in this region of the atmosphere. The adopted chemical rate constant data are from the JPL Publication 19-5 (2020). The diurnal model does not use a family approximation and reactive species O, O_3, N, NO, NO_2, H, OH, HO_2, and H_2O_2 are considered as independent variables. The concentrations of long-lived species are constrained by the results from a two-dimensional chemical transport model (CTM) (Callis et al., 1997). Diffusion coefficients from the CTM are used to parameterize the vertical transport. The diurnal model uses a variable time step, variable order stiff equation solver (Byrne and Hindmarsh, 1975) to integrate the system of species continuity equations. The maximum time step is 600 seconds, and the algorithm automatically reduces the time step to very low values of the order of milliseconds if needed near the terminator. The model is run for 4 diurnal cycles so that the reactive species reach a steady diurnal behavior, and the results from the fifth cycle are used in the analysis. The model is run

for every month at 11 latitudes, corresponding to the latitude nodes of the CTM, from 56.25° N to 56.25°S at an interval of 11.25°.

Calculated O_3 diurnal variation in June at the latitude of 11.25°S and at different altitudes of interest to this work is illustrated in Figure 1. We are restricting our attention to altitudes below 74 km because the SAGE III/ISS O_3 data are noisy in the region above and the quoted uncertainty is also large. O_3 concentration is shown as a function of time starting at midnight. Nighttime O_3 has a constant value representing the total odd oxygen in the lower mesosphere. A sharp decrease at sunrise is mainly caused by photolysis of O_3 forming atomic oxygen. The recombination of atomic oxygen and O_2 quickly balances the loss of O_3 from photolysis. This reaction is pressure dependent and becomes slower at higher altitudes. The photolysis of O_2 generates additional odd oxygen ($O_X = O + O_3$) and in the morning hours this leads to an increase in both O_X and O_3. The formation of odd hydrogen species from the reaction of $O(^1D)$ with H_2O during the day triggers the catalytic destruction of odd oxygen through reactions involving OH. It is noted that between 50 and 80 km the chemical time constant of O_x is of the order of few hours and O_x exhibits a diurnal variation caused by the competing production and destruction reactions. In the early morning there is a net gain of O_X and in the evening there is net loss of O_X, which continues even after sunset until atomic oxygen is depleted. The partitioning of Ox into O and O_3 is mainly controlled by the photolysis of O_3 and the production of O_3 through the recombination of O and O_2. The large increase in O_3 seen around sunset is mainly due to the decrease in the photolysis of O_3 and the continuation of the recombination of O and O_2. O_3 reaches a steady value within an hour or so after sunset. The diurnal model extends to 100 km;

however, since the quoted uncertainty above 70 km in the archived SAGE III/ISS O_3 is large, we will focus on the region below.

The results of the full diurnal cycle are of general interest about the model simulation. But, with reference to solar occultation measurements, the sharp gradients seen in the O_3 concentration near SZA of 90° are more critical. The significance of the twilight variations to the retrieval of mesospheric O_3 under sunrise/sunset conditions can be understood with the help of the schematic shown in Figure 2. This illustrates the occultation geometry in the plane containing the LOS. The red line denotes the LOS at a tangent altitude of Z_T. Points F and N represent the intersection of the LOS with an atmospheric layer at an altitude of Z shown in green. For a species with little or no twilight variations, the concentrations at the locations F and N are nearly equal to that at the location U, the tangent point at an altitude of Z. In this case, the concentrations at tangent height Z_T can be derived in a straightforward manner from the measured transmission using a retrieval algorithm. However, if the photochemistry causes significant gradients near SZA of 90°, as in the case of mesospheric O_3, the distribution around the tangent point becomes nonlinearly asymmetric because the concentrations at F and N depend on the respective local SZA. This variation must be incorporated in the evaluation of O_3 specific optical depth along the LOS.

To illustrate the impact of diurnal variations on slant-path column of O_3, we selected a typical event from the SAGE III/ISS data and applied the calculated O_3 variations in the slant-path column evaluation. The required parameters include month, date, event type (sunrise or sunset), tangent altitude, latitude, longitude, spacecraft latitude and longitude. These data are taken from

158 the current Version 5.2 SAGE III/ISS data available from the Atmospheric Sciences Data Center
159 (ASDC) at NASA Langley Research Center. We used the model results for June at 11.25°S
160 latitude to get the O_3 at sunrise variation along the LOS corresponding to different tangent
161 altitudes from 56 to 76 km. The latitude of the chosen SAGE III/ISS measurement is 11.35°S.
162 The O_3 concentration along the LOS for tangent altitude of 64 km is shown as a function of
163 distance along the LOS relative to the tangent point in the left panel of Figure 3. The dotted line
164 corresponds to the O_3 concentration along the LOS when the diurnal variations are neglected and
165 only the values corresponding to 90° SZA from the layers above the tangent altitude are used.
166 The solid line represents the O_3 including the diurnal variations at the respective altitudes. The
167 increased O_3 concentrations on the instrument side of the LOS are readily seen. The ratio of the
168 O_3 column along the LOS with diurnal variations to the column without the diurnal variations is
169 shown as a function of tangent altitude in the panel on the right side. The peak difference of the
170 order of 30% occurs in the altitude range from 61 to 72 km. Underestimation of the partial O_3
171 slant-path column from layers above the tangent altitude in the standard retrieval translates to
172 overestimation of the retrieved O_3 at the tangent altitude. The bias introduced by the neglect of
173 twilight variations can be evaluated with the help of the diurnal model results.

174

175 The technique is to express the O_3 variation as a function of SZA in terms of concentration
176 normalized to O_3 at SZA of 90°. Figure 4 shows the distribution of the ratio $O_3(\theta)/O_3(\theta=90°)$
177 near sunrise as a function of SZA and altitude obtained from the model results for 11.25°S
178 latitude in June. For a given tangent height, the total slant-path O_3 column comprises of partial
179 slant-path columns corresponding to the layers at and above the tangent height. Spherical
180 geometry dictates that the partial pathlength along the LOS is maximum for the layer

181 immediately above the tangent height (i.e., the lowest layer) and decreases dramatically for
182 higher layers. This, combined with decreasing O_3 concentration with height in the lower
183 mesosphere, results in a total slant-path column dominated by contributions from a few layers
184 right above the tangent point. Therefore, only a small range of SZA, say between 86° and 94°,
185 centered at 90° are important. At 62 km the O_3 ratio is less than 1.0 for SZA less than 90° and it
186 increases gradually for SZA greater than 90°. At higher altitudes, the ratio shows a much steeper
187 increase for SZA greater than 92°. The ratio, in some cases, is even slightly larger than 1.0 at
188 SZA less than 90°. From the occultation geometry shown in Figure 2, it is seen that as one
189 moves away from a SZA of 90° along the LOS at any tangent altitude, the corresponding altitude
190 layer of interest moves upwards. Figure 5 illustrates the O_3 twilight ratio as a function of SZA
191 and altitude for sunset conditions for the same latitude and month. The changes in the ratio for
192 sunset condition are smaller and more gradual especially for SZA greater than 90° compared to
193 the sunrise case. It should be recalled that the daytime variation in the odd oxygen concentration
194 in the lower mesosphere impacts the O_3 concentration differently at sunrise and sunset. The
195 differences between the O_3 variations for sunrise and sunset conditions suggest that the effects on
196 the retrievals are different for sunrise and sunset occultations. The twilight O_3 ratios for altitude
197 layers above the tangent altitude can be used to get the O_3 concentration and hence the optical
198 depth along the LOS more accurately.
199
200 Mesospheric O_3 concentrations are influenced by reactions involving HO_x species and therefore
201 the distribution of H_2O used in the model is an important factor. An earlier study with HALOE
202 mesospheric O_3 data (Natarajan et al. 2005) using the results from the same CTM showed that
203 the monthly, zonal mean H_2O distribution from the CTM was in good agreement with the data

taken from the UARS reference atmosphere project. Linear trend in mesospheric H_2O and solar cycle response have been addressed in literature (Remsberg et al., 2018; Yue et al., 2019). Yue et al. (2019) report a trend in mesospheric H_2O of the order of 4 to 6% per decade based on the data from the Sounding of the Atmosphere using Broadband Emission Radiometry (SABER) and MLS instruments. Long term variability in H_2O certainly impacts the absolute level of mesospheric O_3. But, for the present study, the factor of importance is the relative variation of O_3 very close to SZA of 90° during sunrise and sunset in the mesosphere. We have done a sensitivity study at 11.25° S in June using the diurnal model with a 25% increase in the H_2O concentration. Figure 6 displays the percent change in the twilight O_3 ratios for sunrise shown in Figure 4. The maximum impact below 74 km is less than 20% and it is very small in the lower regions. The twilight ratio in O_3 is quite robust and small changes in the atmospheric parameters such as temperature and H_2O do not impact this ratio much. The use of this ratio is a valid approximation in correcting the retrieval scheme.

3 SAGE III/ISS Mesospheric ozone

The Sage III/ISS instrument payload was launched in February 2017 and successfully attached to the ISS. The ISS occupies a low earth orbit at an inclination of 51.64° that provides occultation coverage of low- and mid-latitude regions. Description of the experiment and early validation of the O_3 measurements are given in McCormick et al. (2020) and Wang et al. (2020). More detailed information on the various wavelength channels and data used for retrieving a suite of atmospheric species including mesospheric O_3 are given in SAGE III Algorithm Theoretical Basis Document (ATBD, 2002) and in the SAGE III/ISS Data Products User's Guide Version

227 3.0 (2021) (DPUG). Among the three different O_3 profile measurements made by the instrument,
228 the one based on short wavelengths in the Hartley-Huggins bands refers exclusively to
229 mesospheric O_3. Three Charge-Coupled Device (CCD) pixel groups (PGs 0-2) are assigned to
230 the short wavelengths in the 280 – 293 nm range, though only one (PG 1 centered at 286 nm) is
231 currently used for the retrieval. According to the DPUG, mesospheric O_3 data have not been
232 fully validated. We also note that the uncertainty in the archived O_3 concentration becomes
233 larger than 10% above 70 km and there are some spurious negative data pointing to uncertainties
234 in the transmission. The present study focusses only on SAGE III/ISS O_3 in the lower
235 mesosphere up to an altitude of 70 km even though the retrieval itself starts at 90 km. The
236 diurnal model described in the previous section extends up to 100km. We use the Version 5.2
237 transmission and species data obtained from ASDC at NASA LaRC. For each year and month,
238 we have categorized the scans according to event type, sunrise, or sunset. The input data for our
239 analysis include the tangent point latitude and longitude, spacecraft latitude and longitude,
240 vertical profiles of neutral density, mesospheric O_3, and transmission. We use only the
241 transmission data from the science pixel group 1 (PG1), which has a center wavelength of
242 286.124 nm, since the predominant species active in this wavelength region is O_3.
243
244 We have generated a database of O_3 twilight ratios for sunrise and sunset conditions from the
245 diurnal model results. These ratios cover for each month the latitude range from 56.25°N to
246 56.25°S at an interval of 11.25°, SZA from 84° to 96° at 0.5° intervals, and altitudes from 56 to
247 90 km at 0.5 km intervals. Using the input data from each of the SAGE III/ISS occultations and
248 spherical geometry relations, for every tangent altitude we compute the SZA as well as partial
249 pathlengths corresponding to overlying layers. This generates a pathlength matrix like the one

used in the standard retrieval. Appropriate O_3 twilight ratios are then obtained by interpolation using the SZA and layer altitude. Multiplication of the standard pathlength matrix by the O_3 ratios yields the modified pathlength matrix including the effects of diurnal variations.

The twilight ratios can either be used to modify the O_3 profiles from the standard retrieval or be incorporated in a new retrieval from measured transmission profile. The first method is like the procedure described by Dubé et al. (2021) for making diurnal corrections to stratospheric NO_2 data from SAGE III/ISS. The archived SAGE III/ISS O_3 profile and the standard pathlength matrix are used to recreate the O_3 specific slant optical depth, as shown by the equation

$$\tau = \sigma S n, \qquad (1)$$

where τ is the O_3 slant optical depth profile, σ is the O_3 cross section corresponding to the center wavelength of PG1, and n is the O_3 profile from the standard retrieval. S represents the pathlength matrix with each row corresponding to a tangent point altitude. This can be written as a triangular matrix because of the geometric symmetry on opposite sides of the tangent point as can be seen from Figure 2. The slant optical depth can then be converted to a O_3 vertical profile corrected for diurnal variations using the modified pathlength matrix described earlier, as shown by the equation

$$n_{wd} = (S_{wd})^{-1} \tau/\sigma = (S_{wd})^{-1} S n \qquad (2)$$

where S_{wd} is the modified pathlength matrix with diurnal correction and n_{wd} is the corrected O_3 profile. Here it is assumed that the O_3 absorption coefficient remains constant along the LOS. This procedure gives a quantitative estimate of the over-prediction by the standard retrieval. The results for a sunrise event on June 14, 2021 (Event ID =2021061438SR) are shown in Figure 7. The left panel displays the O_3 concentration profiles – the solid red line is the archived data from

273 standard retrieval and the solid black line represents the profile after applying the diurnal
274 correction ratios to the pathlength matrix. The percent difference between the standard and the
275 modified profiles is shown by the solid line on the right panel. For this occultation, the difference
276 exceeds 40% above 64 km. This is consistent with the change in O_3 slant column due to the
277 diurnal correction shown in Figure 3. We also note that the retrieval becomes noisy in the upper
278 altitudes as O_3 concentrations reach near detection limits. In the second method, instead of
279 evaluating the slant optical depth using equation 1, the archived slant-path transmission data,
280 which corresponds to PG1, is used along with the standard and modified pathlength matrices to
281 retrieve the vertical O_3 profiles. The change in the slant-path transmission corresponding to the
282 science CCD channel PG1 for each tangent altitude below an upper boundary of 90 km is related
283 to the total slant optical depth made up mainly of O_3 absorption and Rayleigh scattering
284 contributions. After removing the Rayleigh scattering part corresponding to the center
285 wavelength of 286.124 nm, the slant-path O_3 column can be estimated using the O_3 absorption
286 coefficient at this wavelength taken from Bogumil et al. (2003), which is the same database used
287 in the SAGE retrieval algorithm. The standard and modified pathlength matrices are then used to
288 get the vertical O_3 profiles without and with corrections for diurnal variations respectively. The
289 retrieved O_3 profiles for the sunrise event mentioned earlier are given by the dashed lines on the
290 left panel of Figure 7, the red color denoting the standard retrieval without diurnal corrections
291 and the black color the modified retrieval with diurnal corrections. We have used a very simple
292 algorithm and assumed that the transmission data corresponds to a single wavelength to simplify
293 the calculation. The actual retrieval procedure used for the archived products may have included
294 more refinements. The agreement between results of the two different methods is very good,
295 both for the vertical O_3 profiles and for the percent differences. Results for a sunset event, closer

296 to the above sunrise event in location and within a day (Sunset event ID = 2021061515SS) are
297 shown in Figure 8. The impact of the diurnal correction is much smaller for sunset conditions.
298 The maximum difference between the standard and modified profiles is less than 10%. The two
299 different procedures for incorporating diurnal effects yield very nearly same results.
300
301 We have applied the diurnal corrections following the procedure described above to all the
302 SAGE III/ISS measurements from June 2021, categorized by the event type of sunrise or sunset.
303 Individual O_3 profiles were grouped together in 11 latitude bands, 11.25° wide between 56.25°N
304 and 56.25°S. The percent difference between the standard retrieval profile and the corresponding
305 modified profile, defined as $(O_3/O_{3,\,WD} - 1) * 100$, was calculated and the mean for each latitude
306 band was evaluated. The subscript WD refers to the retrieval including the diurnal corrections.
307 Figure 9 shows the resulting distribution of the mean, which represents the over-estimation by
308 the standard retrieval, as a function of latitude and altitude. There is a latitudinal dependence
309 with peak values occurring near 64 km and the summer hemisphere showing smaller difference.
310 Values higher than 100% (dark violet region) are seen in the upper altitudes of the winter
311 hemisphere. The O_3 profile has a sharp gradient reaching a very low minimum in winter between
312 and 70 and 80 km. The retrieved data in this region are very noisy and thus sometimes include
313 negative concentrations. The percent difference between the two retrievals also displays a very
314 noisy distribution with large values of both signs. At altitudes above 85 km, the day-night
315 terminator occurs at solar SZA greater than 96° and O_3 variation around 90° is small. The bias in
316 the standard retrieval (not shown) is also small and there is no need for diurnal correction. The
317 distribution of percent differences for sunset measurements is shown in Figure 10. The values are
318 much smaller as discussed earlier, since the diurnal corrections are not significant for sunset. To

look at the seasonal dependence of the impact of diurnal corrections on the retrieved O_3, we have repeated the procedure with SAGE III/ISS data from January 2021. Figure 11 displays the results for sunrise conditions. The differences between the standard and modified retrievals are larger again in the winter hemisphere with peak values occurring near 64 km. This agrees qualitatively with Figure 11 of Natarajan et al. (2005), which showed the percent difference in retrieved HALOE sunrise O_3 for January 1995 with updated diurnal correction factors compared to the retrieval with HALOE version 19 correction factors. The archived HALOE version 19 retrieval used correction factors from a diurnal calculation at 61 km for all mesospheric tangent altitudes above. Since a partially corrected (version 19) retrieval was used as the basis, the contour levels are negative and smaller in magnitude.

4 Comparisons with other measurements

It is of interest to see whether the correction to the retrieval of mesospheric ozone described above can be validated by comparisons with other independent measurements. Mesospheric ozone mixing ratios at SZA of 90° during sunrise and sunset have been measured by other solar occultation experiments like HALOE and ACE-FTS. HALOE version 19 retrievals use correction factors based on diurnal model calculation near the stratopause. An update to these correction factors was discussed in Natarajan et al. (2005) but a modified version of the full ozone dataset was not generated. As far as we know, the retrieval scheme of ACE-FTS does not use any correction for twilight variations of mesospheric ozone. It should be emphasized that comparisons with data from other solar occultation experiments do not necessarily provide a

robust independent validation of the need to make such corrections to reduce the bias in the measurements.

MLS aboard the Aura satellite also provides vertical profiles of O_3 extending into the mesosphere. MLS measurements occur twice a day, once in the early afternoon and the other past midnight. Strode et al. (2022) have used the MLS data scaled with factors derived from Goddard Earth Observing System (GEOS) model coupled with the Global Modeling Initiative (GMI) chemistry mechanism for comparisons with SAGE III/ISS O_3 in the stratosphere. We have done similar comparisons for a selected subset of the data in the lower mesosphere using the results from the mesospheric diurnal model described earlier. We limited our attention to the data in altitude range from 56 to 70 km. We used the information provided in the MLS-V5 data quality document (Livesey et al., 2022) to properly screen the O_3 data. The vertical resolution for MLS O_3 varies from 3 to 5.5 km in the lower mesosphere. The reported accuracy varies from 8% at 0.21 hPa to 40% at 0.02 hPa. We used the MLS V-5 O_3 profiles from a 11.25° latitude band centered at 11.25° S from June 13 to June 15 of 2021. The native units of MLS measurements are mixing ratios on pressure levels. We used the MLS temperature and geopotential height data to get O_3 concentrations on an altitude grid. We derived the mean and the standard deviation profiles for both day and night MLS measurements. Results from diurnal model calculations were used to convert MLS day and night measurements to SZA of 90 ° during sunrise and sunset conditions. Figure 12 shows the O_3 concentration at sunrise based on MLS night data by asterisks and that based on MLS day data by diamonds. The horizontal lines represent the standard deviations at different altitudes. We also obtained the mean and standard deviation profiles from SAGE III/ISS data the same latitude band and period in June 2021 like the selected

MLS data. The solid black line in the figure shows the mean sunrise profile from standard retrieval and the standard deviation is represented by the yellow color band. The dashed black line is the modified retrieval with the green band showing the standard deviation. The twilight corrections to the mesospheric O_3 retrieval brings the profile in better agreement with that derived from MLS day and night data. Above 68 km the MLS day measurements have large variability, and the standard deviation is larger than the mean. Figure 13 shows the comparison of the profiles for sunset conditions. The difference between the modified and the standard retrievals is much smaller for the sunset conditions compared to the sunrise condition. Overall SAGEIII/ISS mesospheric O_3 has a positive bias. The vertical resolution of SAGE III/ISS data is about 0.7 km which is finer than the MLS vertical resolution. We found that the application of the MLS O_3 averaging kernel to smooth the SAGE III/ISS data has a minimum impact on the comparison.

There have been several ground-based microwave measurements of atmospheric O_3 and its diurnal variations (Connor et al., 1994; Parrish et al., 2014; Sauvageat et al., 2022). The microwave radiometry (MWR) in Switzerland (Sauvageat et al., 2022) provides data temporally overlapping the SAGE III/ISS data. These data are from measurements made at 2 ground stations and they extend into the mesosphere. The vertical resolution of ground based MWR is very coarse in the lower mesosphere, about 17 km (Connor et al., 1994). Therefore SAGE III/ISS O_3 data should be convolved with the averaging kernels of MWR prior to comparisons. In addition, MWR provides hourly data and, unless the local measurement time coincides with SZA of 90° during sunrise and sunset, the data must be converted using factors based on diurnal model. We feel that comparison with MWR data is outside the scope of this paper.

5 Sunrise to Sunset Ratio

Brühl et al. (1996), in their paper on HALOE O_3 channel validation, discussed the sunrise to sunset differences in O_3 around 0.1 hPa (about 64 km). Mesospheric layers are under sunlit conditions even at SZA slightly greater than 90° at dawn and dusk. As explained earlier, the viewing geometry in solar occultation observations leads to an increase in the contribution of overlying layers to the O_3 optical depth because O_3 concentrations corresponding to varying SZA greater than 90° are seen along the LOS. We have noted that the impact is larger during sunrise than sunset measurement. The sunrise to sunset O_3 concentration ratio becomes larger if the diurnal variations along the LOS are not considered in the retrieval. Solar occultation experiments occasionally offer the opportunity to approximately check this ratio as a test of consistency of measurement and agreement with theory. This is possible when sunrise and sunset orbits cross over each other within a reasonably short interval of time and physical proximity. Such near coincidences are quite rare. We selected sunrise/sunset pairs of measurements by SAGE III/ISS having tangent locations within 1.5° latitude, and 15° longitude of each other and separated by a maximum of 36 hours. The effect of advection by the prevailing westerly wind requires that the time and longitude differences are in the correct direction. There are just 10 pairs of sunrise /sunset measurements in June 2021 that satisfy the above criteria, all of them in low latitudes with a mean latitude of 10.46°S at sunrise and 10.27°S at sunset. The mean of the sunrise to sunset ratios of O_3 concentrations for these 10 scans is shown in Figure 14. The solid line corresponding to the standard retrieval shows ratios greater than 1.1 above 60 km. The green color shade represents the standard deviation. The modified retrieval yields a ratio

shown by the dashed line decreasing from 1.01 at 60 km to lower values above. The horizontal lines are the standard deviations. The asterisk symbols represent the ratio from the diurnal model. The model value is in good agreement with the ratios from both the standard and modified retrievals near 58 km but above this altitude there is some difference. The variation with altitude in the model ratio is more like that shown by the modified retrieval. The modified retrieval qualitatively reflects the pattern that photochemistry of O_3 suggests in this altitude region. This comparison serves as an independent criterion to highlight the importance of including the LOS twilight variations in the retrieval of mesospheric O_3 in solar occultation measurements. We noticed that very few such pairs of measurements, which satisfied the criteria we have chosen, occurred during other months in SAGE III/ISS data. We have also looked at the latitudinally averaged sunrise and sunset data for June 2021 obtained for generating figures 9 and 10. For the latitude band centered at 11.25° S, the sunrise to sunset ratio as a function altitude (not shown) is like Figure 14, which used only collocated data. The small sampling size of the collocated pairs of data and regions of overlapping standard deviations seen in the Figure 14 make this at best an approximate comparison. Other independent measurements are needed to verify the altitude variation of the ratio of sunrise to sunset O_3 concentrations.

6 Summary

Photochemically induced changes in species concentration at twilight can cause asymmetries in the distribution along the LOS of a solar occultation observation, variations that must be considered in the retrieval algorithm. Prominent among the species that need corrections for twilight variations are NO and NO_2 in the stratosphere and O_3 in the mesosphere. The SAGE

III/ISS instrument uses the measurements in the short-wave Hartley-Huggins band to get mesospheric O_3 profiles. The standard retrieval procedure does not consider the LOS variations in O_3 caused by photochemistry. This study describes a procedure to use results from diurnal photochemical model simulations to develop correction factors for different altitudes, latitudes, and months. These factors were used along with the archived SAGE III/ISS mesospheric O_3 data for selected time periods to obtain modified O_3 profiles. For the month of June 2021, it is shown that neglecting the diurnal variations can result in nearly 50% overestimation of O_3 at 64 km at lower latitudes. An approximate retrieval using the transmission data from SAGE III/ISS also indicates similar behavior in the profiles obtained with and without diurnal corrections. The retrievals were repeated for January 2021 to study the seasonal impact. Larger differences are generally seen near 70 km in high latitude winter hemisphere, and this is most likely due to a combination of very low O_3 concentrations, large twilight correction factors, and large uncertainties in the data. The results from this study are in good agreement with those obtained for the retrieval of HALOE mesospheric O_3 data.

SAGE III/ISS data include a few nearly collocated sunrise and sunset measurements, mostly in the low latitudes and about a day apart. There are 10 pairs of such sunrise and sunset measurements in June 2021. An analysis of the sunrise to sunset ratio profile from these data indicates that the retrievals that include the diurnal variations show qualitatively better agreement with theoretical prediction.

Data Availability

SAGE III/ISS version 5.2 data is available from https://asdc.larc.nasa.gov/project/SAGE%20III-ISS/g3bssp_52. MLS O_3 data are available from https://disc.gsfc.nasa.gov/. O_3 twilight ratios used in this study are available from the author. They can also be obtained from any diurnal photochemical model of the mesosphere.

Author Contribution

MN conducted the photochemical model calculations, SAGE III/ISS O_3 retrievals, and the analyses described in the study, and he wrote the manuscript. RD and DF provided information and guidance on the use of SAGE III/ISS mesospheric O_3 data as well as comments on the manuscript.

Competing Interests

The authors declare that there is no competing interest for this study.

Acknowledgements

SAGE III/ISS data used in this study were obtained from the NASA Langley Research Center Atmospheric Science Data Center. MN carried out this work while serving as a Distinguished Research Associate of the Science Directorate at NASA Langley Research Center. MN thanks Ellis Remsberg for reading and commenting on the draft version of this manuscript.

References

Bogumil, K., Orphal, J., Homann, S., Voigt, P., Spietz, O., Fleischmann, A., Vogel, M., Hartmann, H., Bovensmann, J., Frerick, J., and Burrows, J.: Measurements of molecular absorption spectra with the SCIAMACHY pre-flight model: instrument characterization and reference data for atmospheric remote sensing in the 230-2380 nm region, J. Photochemistry and Photobiology A: Chemistry, Vol 157, No. 2-3, 167-184, 2003.

Boughner R. E., Larsen, J. E., and Natarajan., M.: The influence of NO and ClO variations at twilight on the interpretation of solar occultation measurements, Geophys. Res. Lett., 7, 231 – 234, 1980.

Brohede, S. M., Haley, C. S., McLinden, C. A., Sioris, C. E., Murtagh, D. P., Petelina, S. V., Llewellyn, E. J., Bazureau, A., Goutail, F., Randall, C. E., Lumpe, J. D., Taha, G., Thomasson, L. W., and Gordley, L. L.: Validation of Odin/OSIRIS stratospheric NO_2 profiles, J. Geophys. Res.-Atmos., 112, D07310, https://doi.org/10.1029/2006JD007586, 2007.

Brühl, C., Drayson, S. R., Russell III, J. M., Crutzen, P. J., McInerney, J. M., Purcell, P. N., Claude, H., Gernandt, H., McGee, T. J., McDermid, I. S., and Gunson, M. R.: Halogen Occultation Experiment ozone channel validation, J. Geophys. Res., Vol. 101, NO. D6, 10,217 - 10,240, 1996.

Byrne, G. D., and Hindmarsh, A. C.: A polyalgorithm for the numerical solution of ordinary differential equations, ACM Trans. Math. Soft., 1(1), 71-96, 1975.

Connor, B. J., Siskind, D. E., Tsou, J. J., Parrish, A., and Remsberg, E. E.: Ground-based microwave observations of ozone in the upper stratosphere and mesosphere, J. Geophys. Res., vol 99, No. D8, 16,757-16,770, 1994.

Dubé, K., Bourassa, A., Zawada, D., Degenstein, D., Damadeo, R., Flittner, D., and Randel, W.: Accounting for the photochemical variation in stratospheric NO_2 in the SAGE III/ISS solar

500 occultation retrieval, Atmos. Meas. Tech., 14, 557 – 566, https://doi.org/10.5194/amt-14-557-
501 2021, 2021.

502 Gordley, L. L., Russell III, J. M., Mickley, L. J., Frederick, J. E., Park, J. H., Stone, K. A.,
503 Beavee, G. M., McInerney, J. M., Deaver, L. E., Toon, G. C., Murcray, F. J.,Blatherwick, R. D.,
504 Gunson, M. R., Abbatt, J. P. D., Mauldin III, R. L., Mount, G. H., Sen, B., and Blavier, J. F.:
505 Validation of nitric oxide and nitrogen dioxide measurements made by the Halogen Occultation
506 Experiment for UARS platform, J. Geophys. Res.-Atmos., 101,10241–10266, 1996.

507 JPL Publication 19-5, Chemical Kinetics and Photochemical Data for Use in Atmospheric
508 Studies, Evaluation Number 19. https://jpldataeval.jpl.nasa.gov/pdf/NASA-
509 JPL%20Evaluation%2019-5.pdf, 2020.

510 Livesey, N. J., Read, W. G., Wagner, P. A., Froidevaux, L., Santee, M. L., Schwartz, M. J.,
511 Lambert, A., Millan Valle, L. F., Pumphrey, H. C., Manney, G. L., Fuller, R. A., Jarnot, R. F.,
512 Knosp, B. W., and Lay, R. R.: Earth Observing System (EOS) Aura Microwave Limb Sounder
513 (MLS) Version 5.0x Level 2 and 3 data quality and description document, JPL D-105336 Rev B,
514 2022.

515 McCormick, M. P., Lei, L., Hill, M. T., Anderson, J., Querel, R., and Steinbrecht, W.: Early
516 results and validation of SAGE III-ISS ozone profile measurements from onboard the
517 International Space Station, Atmos. Meas. Tech., 13, 1287-1297, https://doi.org/10.5194/amt-13-
518 1287-2020, 2020.

519 Natarajan, M., Deaver, L. E., Thompson, E., and Magill, B.: Impact of twilight gradients on the
520 retrieval of mesospheric ozone from HALOE, J. Geophys. Res., Vol. 110,
521 doi:10.1029/2004JD005719, 2005.

Newchurch, M. J., Allen, M., Gunson, M. R., Salawitch, R. J., Collins, G. B., Huston, K. H., Abbas, M. M., Abrams, M. C., Chang, A. Y., Fahey, D. W., Gao, R. S., Irion, F. W., Loewenstein, M., Manney, G. L., Michelson, H. A., Podolske, J. R., Rinsland, C. P., and Zander, R.: Stratospheric NO and NO_2 abundances from ATMOS Solar-Occultation Measurements, Geophys. Res. Lett., 23, 2373-2376., https://doi.org/10.1029/96GL01196,1996.

Parrish, A., Boyd, I. S., Nedoluha, G. E., Bhartia, P. K., Firth, S. M., Kramarova, N. A., Connor, B. J., Bodeker, G. E., Froidevaux, L., Shiotani, M., and Sakazaki, T.: Diurnal variations of stratospheric ozone measured by ground-based microwave remote sensing at the Mauna Loa NDACC site: measurement validation and GEOSCCM model comparison, Atmos. Chem. Phys., 14, 7255-7222, www.atmos-chem-phys.net/14/7255/2014/doi:10.5194/acp-14-7255-2014, 2014

Remsberg, E., Damadeo, R., Natarajan, M., and Bhatt, P.: Observed responses of mesospheric water vapor to solar cycle and dynamical forcings, J. Geophys. Res., 123 (7), 3830-3843, https://doi.org/10.1002/2017JD028029, 2018.

Russell III, J. M., Farmer, C. B., Rinsland, C. P., Zander, R., Froidevaux, L., Toon, G. C., Gai, B., Shaw, J., and Gunson, M.: Measurements of Odd Nitrogen Compounds in the Stratosphere by the ATMOS Experiment on Spacelab 3, J. Geophys. Res., Vol 3, D2, 1718-1736, 1988.

Sauvageat, E., Barras, E. M., Hocke, K., Haefele, A., and Murk, A.: Harmonized retrieval of middle atmospheric ozone from two microwave radiometers in Switzerland, https://doi.org/10.5194/amt-2022-212, 2022

SAGE III Algorithm Theoretical Basis Document (ATBD) Solar and Lunar Algorithm, LaRC 475-00-109, Version 2.1. https://eospso.gsfc.nasa.gov/sites/default/files/atbd/atbd-sage-solar-lunar.pdf, 2002

SAGE III/ISS Data Products User's Guide, Version 3.0, https://asdc.larc.nasa.gov/documents/sageiii-iss/guide/DPUG-G3B-2-0.pdf, 2021.

Strode, S. A., Taha, G., Oman, L. D., Damadeo, R., Flittner, D., Schoeberl, M., Sioris, C. E., and Stauffer, R.: SAGE III/ISS ozone and NO_2 validation using diurnal scaling factors, https://doi.org/10.5194/amt-15-6145-2022, Atmos. Meas. Tech., 15, 6145-6161, 2022

Wang, H. J. R., Damadeo, R., Flittner, D., Kramarova, N., Taha, G., Davis, S., et al.: Validation of SAGE III/ISS solar occultation ozone products with correlative satellite and ground-based measurements, J. Geophys. Res., 125, e2020JD032430. https://doi.org/10.1029/2020JD032430, 2020.

Yue, J., Russell III, J., Gan, Q., Wang, T., Rong, P., Garcia, R., and Mlynczak, M.:Increasing water vapor in the stratosphere and mesosphere after 2002, Geophys. Res. Lett., 46, 13,452-13,460. https://doi.org/10.1029/2019GL084973, 2019.

Appendix

Photochemical reactions considered in the mesospheric diurnal model:

(1) $O_2 + h\upsilon \rightarrow O + O$

(2) $O_3 + h\upsilon \rightarrow O + O_2$

(3) $O_3 + h\upsilon \rightarrow O(^1D) + O_2$

(4) $NO_2 + h\upsilon \rightarrow O + NO$

(5) $H_2O + h\upsilon \rightarrow OH + H$

(6) $H_2O_2 + h\upsilon \rightarrow OH + OH$

(7) $NO + h\upsilon \rightarrow N + O$

(8) $H_2O + h\upsilon \rightarrow H_2 + O$

(9) $O(^1D) + O_2 \rightarrow O + O_2$

(10) $O(^1D) + N_2 \rightarrow O + N_2$

(11) $O(^1D) + H_2O \rightarrow OH + OH$

(12) $O + O + M \rightarrow O_2 + M$

(13) $O + O_2 + M \rightarrow O_3 + M$

(14) $O + O_3 \rightarrow O_2 + O_2$

(15) $O + OH \rightarrow H + O_2$

(16) $O + HO_2 \rightarrow OH + O_2$

(17) $NO_2 + O \rightarrow NO + O_2$

(18) $H + O_2 + M \rightarrow HO_2 + M$

(19) $O_3 + OH \rightarrow HO_2 + O_2$

(20) $O_3 + NO \rightarrow NO_2 + O_2$

(21) $O_3 + H \rightarrow OH + O_2$

(22) $OH + HO_2 \rightarrow H_2O + O_2$

(23) $HO_2 + NO \rightarrow OH + NO_2$

(24) $OH + H_2O_2 \rightarrow H_2O + HO_2$

(25) $HO_2 + HO_2 \rightarrow H_2O_2 + O_2$

(26) $HO_2 + O_3 \rightarrow OH + 2\ O_2$

(27) $O(^1D) + H_2 \rightarrow OH + H$

(28) $N + O_2 \rightarrow NO + O$

(29) $N + NO \rightarrow N_2 + O$

(30) $N + NO_2 \rightarrow N_2O + O$

(31) $H + HO_2 \rightarrow OH + OH$

(32) $H + HO_2 \rightarrow H_2O + O$

(33) $H + HO_2 \rightarrow H_2 + O_2$

(34) $OH + H_2 \rightarrow H_2O + H$

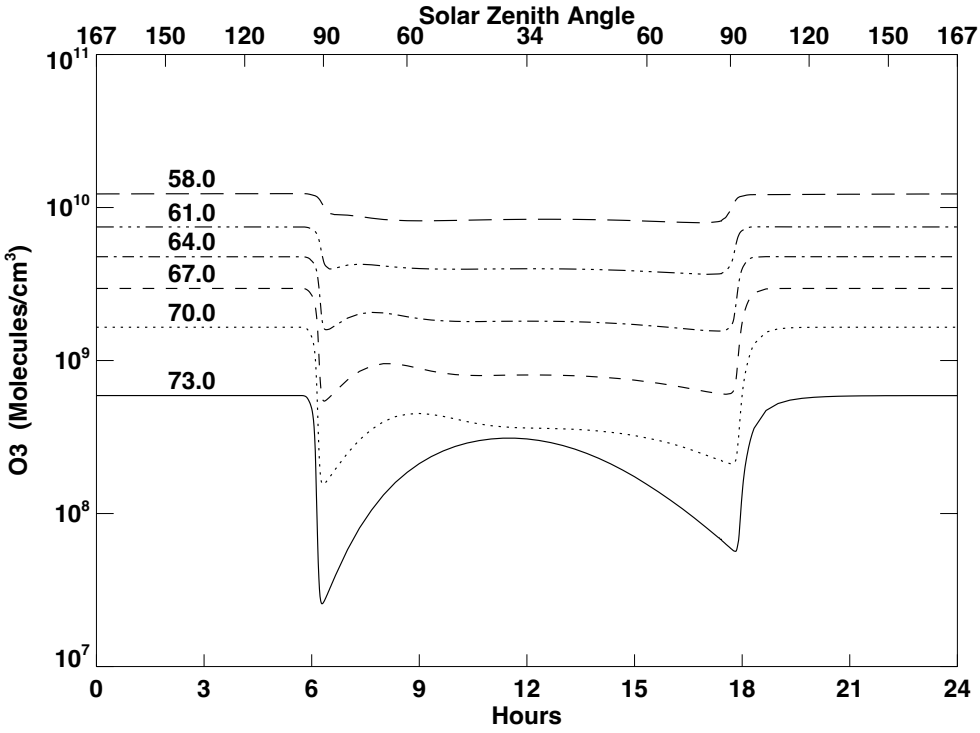

598

599

600 Figure 1. Diurnal variation in O_3 at 11.25°S in June at altitudes from 58 to 73 km. 0 hours

601 denote midnight. The upper X axis shows the variation of SZA.

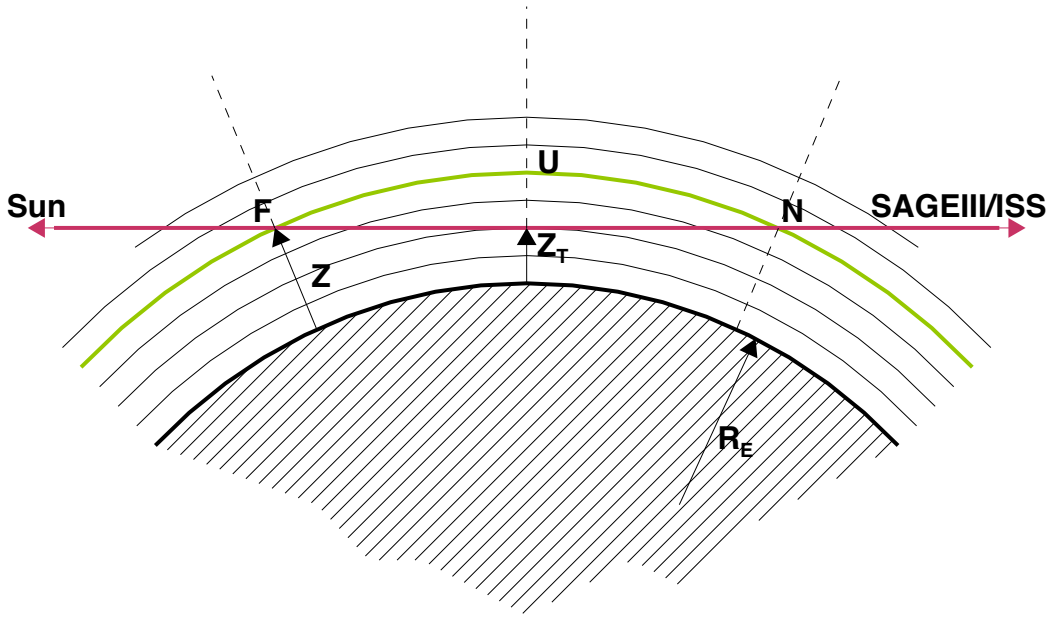

602

603 Figure 2. Schematic representation of the solar occultation measurement. Z_T is the tangent

604 altitude, red line is the LOS, Z is the altitude of a layer above the tangent altitude, F (towards

605 sun) and N (towards SAGE III/ISS) are the points of intersection of layer at Z with the LOS, and

606 R_E is the earth radius.

607

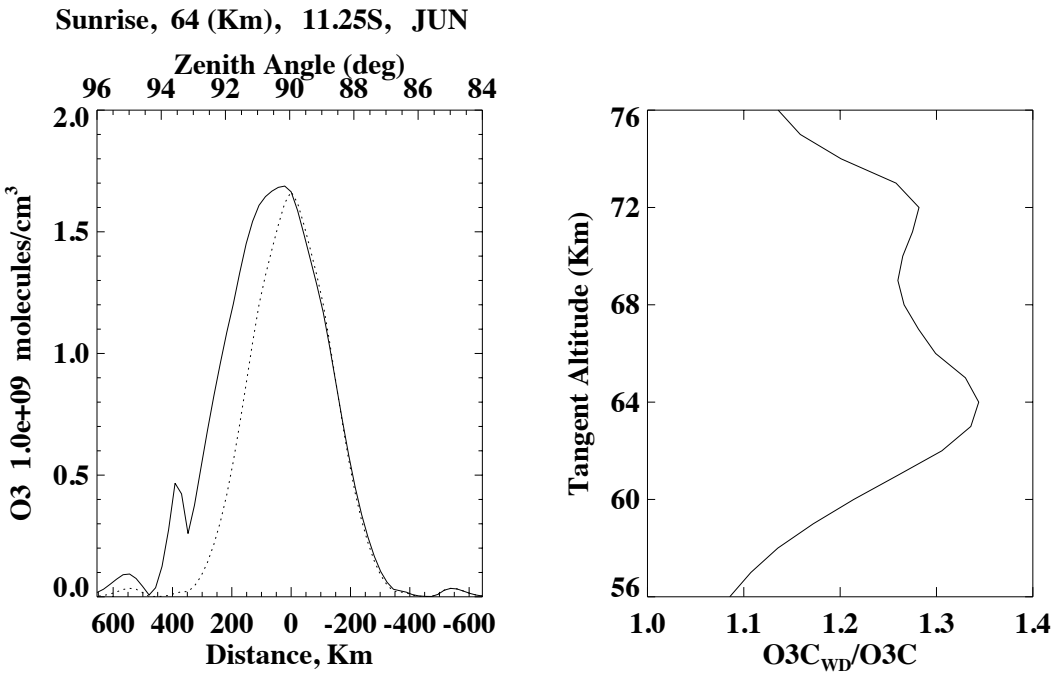

608

609 Figure 3. (Left) O_3 concentration along the LOS for a tangent altitude of 64 km at sunrise
610 at11.25°S latitude in June. Solid line shows O_3 with diurnal variations and the dotted line
611 represents O_3 without diurnal variations. The X-axis represents the distance along the LOS
612 relative to the tangent point with positive direction towards the instrument and negative direction
613 towards the Sun. The upper axis shows the corresponding SZA. (Right) Ratio of the O_3 column
614 along the LOS with appropriate diurnal variations to the O_3 column without diurnal variations,
615 plotted as a function of altitude at 11.25°S in June.

616

617

618

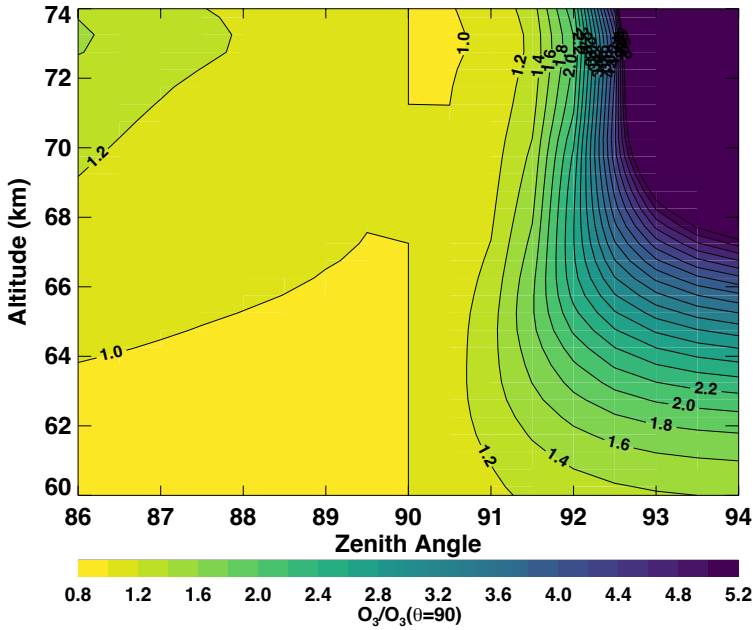

619

620 Figure 4. Ozone twilight ratio, defined as O_3 at solar zenith angle θ/O_3 at $\theta=90°$, as a function of

621 SZA and altitude for sunrise in June and 11.25°S latitude.

622

623

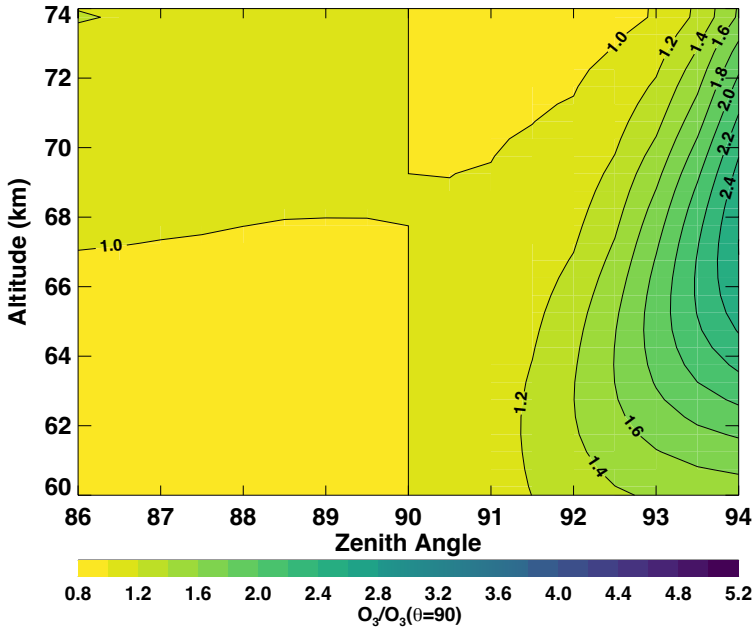

624

625 Figure 5. Ozone twilight ratio, defined as O_3 at solar zenith angle θ/O_3 at $\theta=90°$, as a function of

626 SZA and altitude for sunset in June and 11.25°S latitude.

627

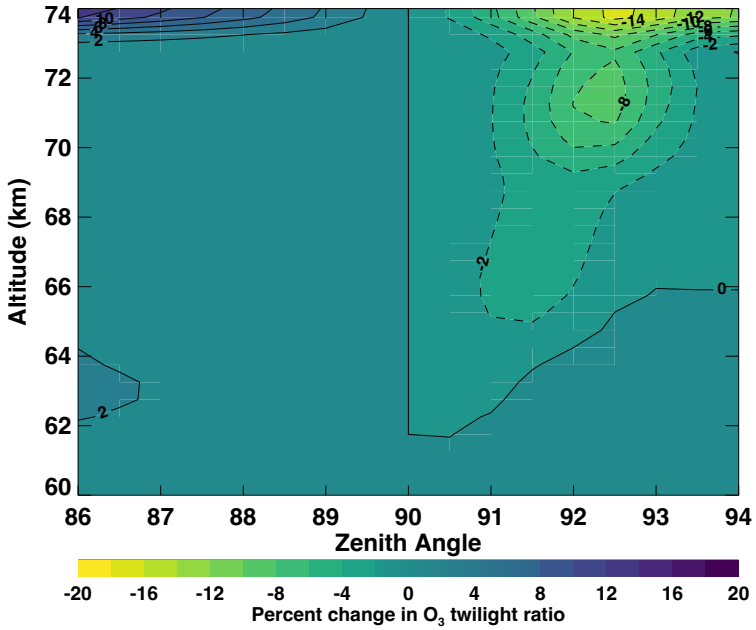

628

629 Figure 6. Percent change in the O_3 twilight ratio shown in Figure 4 when the H_2O in the diurnal

630 model is increased by 25% at all altitudes. This figure corresponds to sunrise at 11.25° S in June.

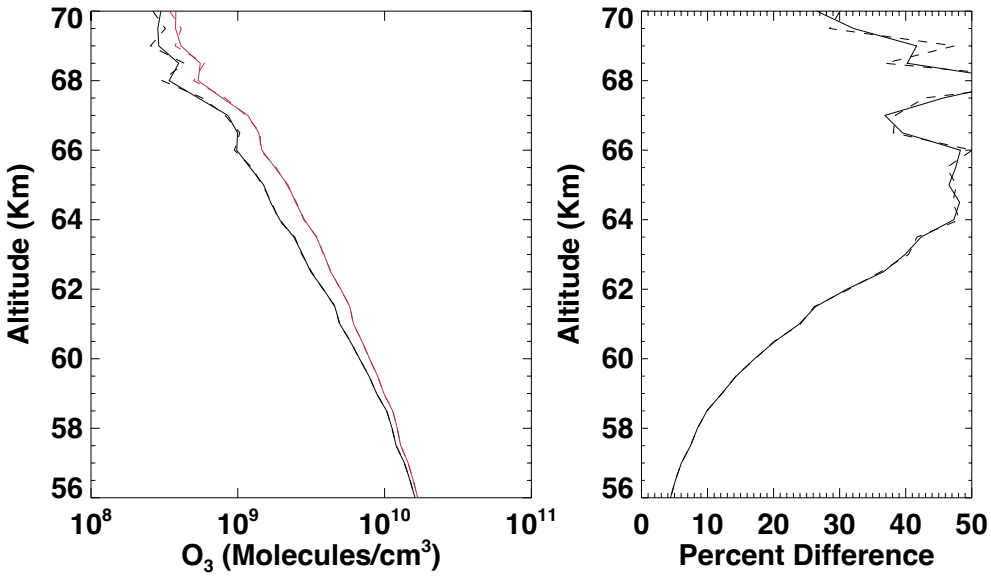

631

632 Figure 7. SAGE III/ISS O_3 for a sunrise event at 11.35°S and 158.72°E on June 14, 2021 (Event
633 ID 2021061438SR). (Left panel) Red solid line shows the standard SAGE III retrieval, and the
634 black solid line represents the retrieval including the diurnal variations along LOS. The dashed
635 lines represent the retrievals using the transmission data, the red color for the standard retrieval
636 and the black denoting the retrieval with diurnal corrections. (Right panel) Percent difference
637 between the standard retrieval and the one with diurnal corrections; solid line using the archived
638 standard retrieval of O_3 concentration, and the dashed line based on the approximate retrieval
639 using the transmission data.

640

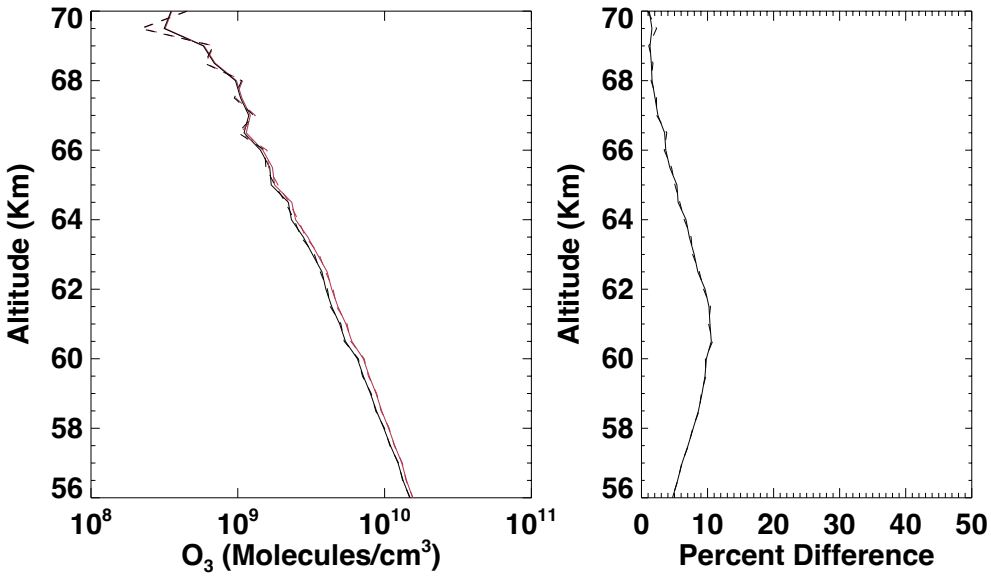

641

642 Figure 8. SAGE III/ISS O_3 for a sunset event at 12.05°S and 151.16°E on June 15, 2021 (Event
643 ID 2021061515SS). (Left panel) Red solid line shows the standard SAGE III retrieval, and the
644 black solid line represents the retrieval including the diurnal variations along LOS. The dashed
645 lines represent the retrievals using the transmission data, the red color for the standard retrieval
646 and the black denoting the retrieval with diurnal corrections. (Right panel) Percent difference
647 between the standard retrieval and the one with diurnal corrections; solid line using the archived
648 standard retrieval of O_3 concentration, and the dashed line based on the approximate retrieval
649 using the transmission data.

650

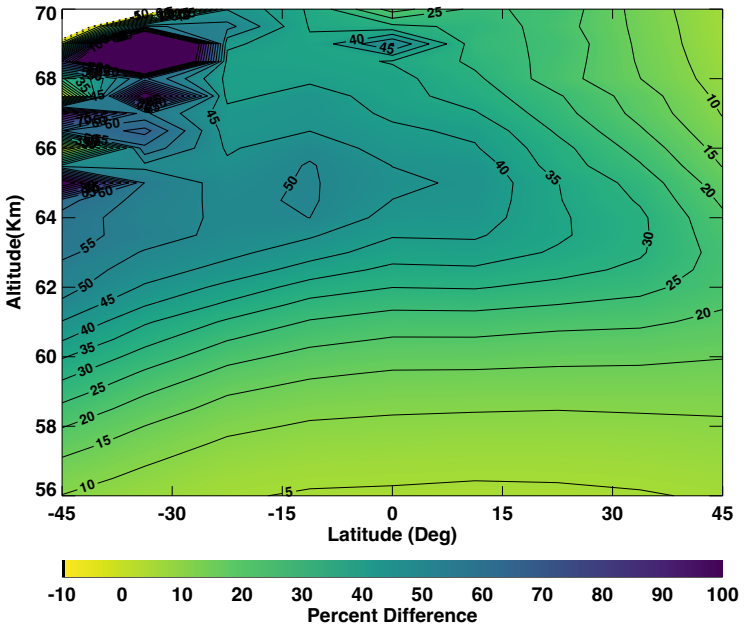

Figure 9. Latitudinal average of the percent difference in sunrise O_3 between the standard (archived) retrieval and a retrieval including diurnal variations along the LOS, as a function of latitude and altitude for June 2021.

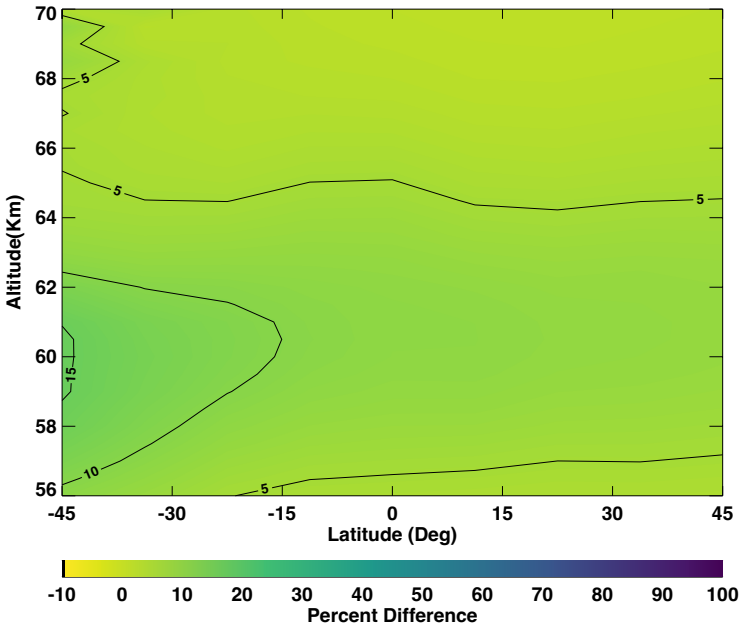

657

658 Figure 10. Latitudinal average of the percent difference in sunset O_3 between the standard

659 (archived) retrieval and a retrieval including diurnal variations along the LOS, as a function of

660 latitude and altitude for June 2021.

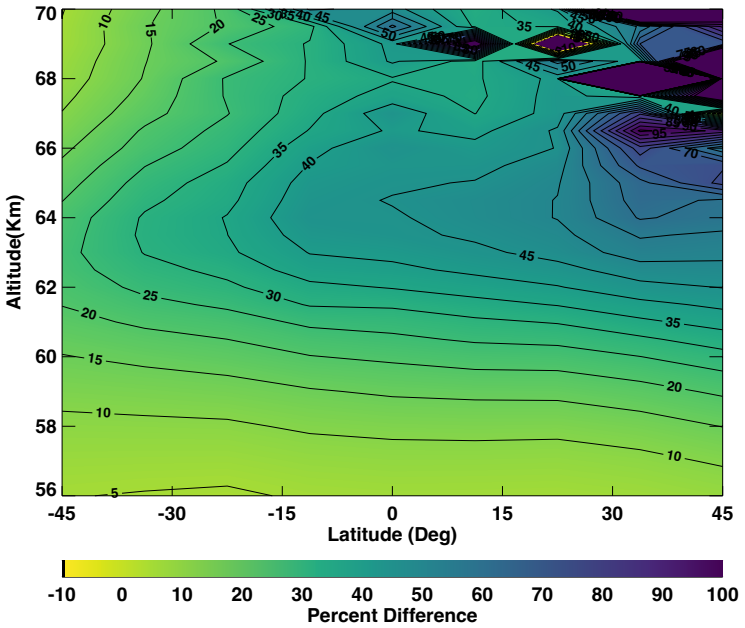

661

662 Figure 11. Latitudinal average of the percent difference in sunrise O_3 between the standard

663 (archived) retrieval and a retrieval including diurnal variations along the LOS, as a function of

664 latitude and altitude for January 2021.

665

666

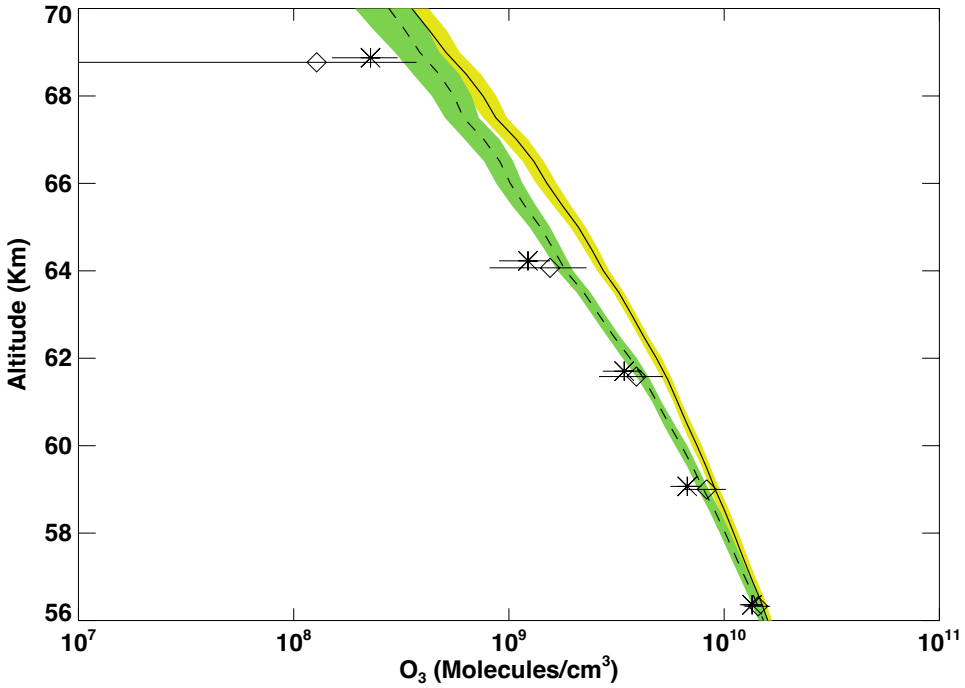

667

668 Figure 12. Comparison of sunrise SAGE III/ISS and MLS mesospheric O_3 zonal mean at 11.25°
669 S in June 2021. Solid line – mean of SAGE III/ISS standard retrieval with the standard deviation
670 shown by the yellow shade; Dashed line – mean of SAGE III/ISS modified retrieval with the
671 standard deviation shown by the green shade; Asterisks – mean MLS night data scaled to
672 sunrise; Diamonds – mean MLS day data scaled to sunrise; Horizontal lines represent the
673 standard deviations.

674

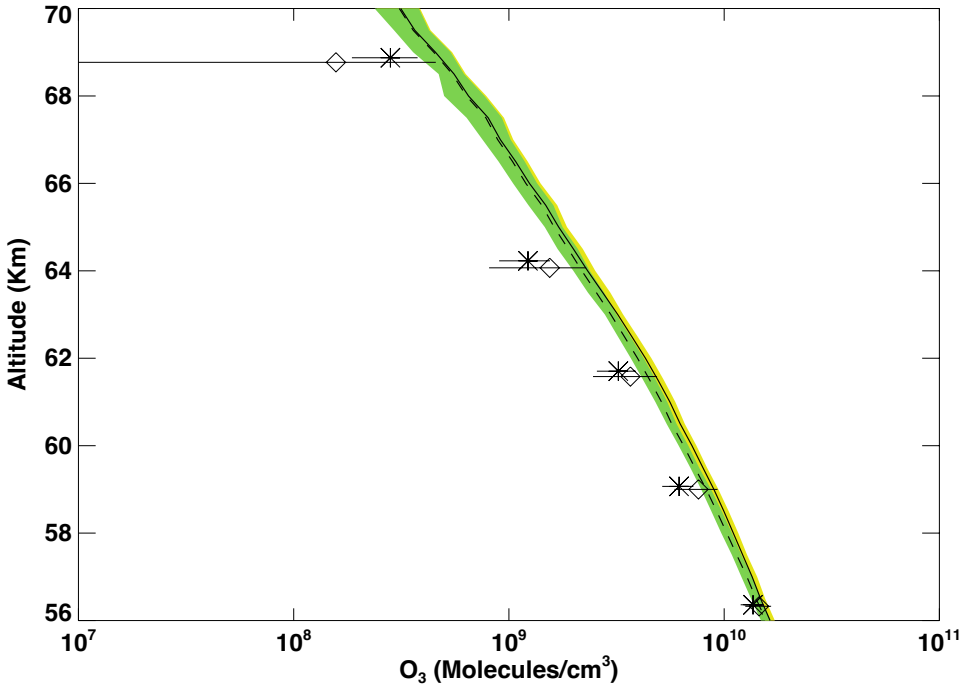

675

676 Figure 13. Comparison of sunset SAGE III/ISS and MLS mesospheric O_3 zonal mean at 11.25°
677 S in June 2021. Solid line – mean of SAGE III/ISS standard retrieval with the standard deviation
678 shown by the yellow shade; Dashed line – mean of SAGE III/ISS modified retrieval with the
679 standard deviation shown by the green shade; Asterisks – mean MLS night data scaled to sunset;
680 Diamonds – mean MLS day data scaled to sunset; Horizontal lines represent the standard
681 deviations.

682

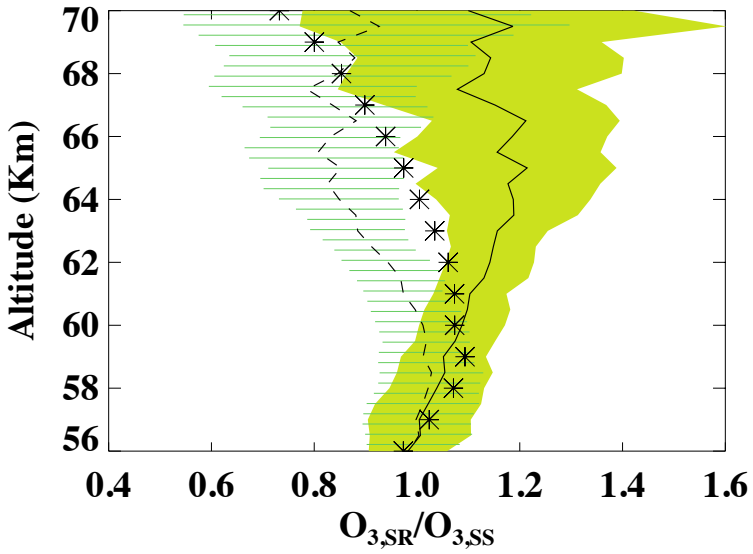

683

684 Figure 14. Vertical profile of O_3 sunrise to sunset ratio in June 2021. Nearly collocated 10 pairs
685 of sunrises (mean latitude 10.46°S) and sunsets (mean latitude 10.27°S) data are used for this
686 plot. Solid line shows the mean ratio from standard (archived) retrieval and the green shade
687 represents the standard deviation; Dashed line shows the mean ratio from the retrieval including
688 diurnal variations along the LOS and the horizontal lines represent the standard deviation. The
689 asterisk symbols are the ratios from diurnal photochemical calculations at 11.25°S for June.